Thermodynamic Characterization of the Protein−Protein Interaction in the Heteromeric *Bacillus subtilis* Pyridoxalphosphate Synthase†

Martina Neuwirth,‡,§ Karlheinz Flicker,‡,§ Marco Strohmeier,|| Ivo Tews,|| and Peter Macheroux*,‡

Institut für Biochemie, Technische Universität Graz, Petersgasse 12/2, A-8010 Graz, Austria, and Biochemiezentrum der Universität Heidelberg, Im Neuenheimer Feld 328, D-69120 Heidelberg, Germany

Received December 19, 2006; Revised Manuscript Received February 21, 2007

ABSTRACT: Two biosynthetic routes for the synthesis of pyridoxal 5′-phosphate (PLP), the biologically active compound of vitamin B6, have been characterized. The major pathway leads to direct formation of PLP from a pentasaccharide and a trisaccharide and is operative in plants, fungi, protozoa, and bacteria. This reaction is catalyzed by a single glutamine amidotransferase enzyme complex consisting of a pyridoxal synthase, termed Pdx1, and a glutaminase, termed Pdx2. In this complex, Pdx2 generates ammonia from L-glutamine and supplies it to Pdx1 for incorporation into PLP. The glutaminase activity of Pdx2 requires the presence of Pdx1 in a heteromeric complex, previously characterized by a crystallographic three-dimensional (3D) structure determination. Here, we give a thermodynamic description of complex formation of *Bacillus subtilis* PLP synthase in the absence or presence of L-glutamine. We show that L-glutamine directly affects the tightness of the protein complex, which exhibits dissociation constants of 6.9 and 0.3 μM in its absence and presence, respectively (at 25 °C). This result relates to the positioning of L-glutamine on the heterodimer interface as seen in the 3D structure. In an analysis of the temperature dependence of the enthalpy, negative heat capacity changes (ΔC_p) agree with a protein interface governed by hydrophobic interactions. The measured heat capacity change is also a function of L-glutamine, with a negative ΔC_p in the presence of L-glutamine and a more negative one in its absence. These findings suggest that L-glutamine not only affects the strength of complex formation but also determines the forces involved in complex formation, with regard to different relative contributions of hydrophobic and hydrophilic interactions.

Vitamin B6 serves as an essential cofactor in many enzymatic reactions such as transaminations and decarboxylations in amino acid metabolism (*1*, *2*). Its biosynthesis is restricted to bacteria, protozoa, fungi, and plants, whereas animals and humans require a constant supply of the vitamin in their diet. The biosynthesis of vitamin B6 has been studied extensively in the bacterial model organism *Escherichia coli*, leading to the complete discovery of the chemical steps and the enzymes involved in the required transformations (*3*, *4*). Until a few years ago, it was believed that the *de novo* biosynthesis of vitamin B6 follows the same chemical pathway in all other organisms capable of its biosynthesis. The discovery of an alternative vitamin B6 biosynthetic pathway in the fungus *Cercospora nicotianae* has shed doubt on the current hypothesis of a single biosynthetic pathway (*5*, *6*). Phylogenetic analyses of genomic data from prokaryotes and unicellular eukaryotes have confirmed the occurrence of homologous genes implicated in the alternative vitamin B6 pathway in most species except for the γ subdivision of proteobacteria (*7*), suggesting that the *E. coli* biosynthetic pathway is the exception rather than the rule for de novo biosynthesis of vitamin B6. More recently, experimental studies have proven that the alternative pathway is in operation in such diverse organisms as the yeast *Saccharomyces cerevisiae*, the Gram-positive bacterium *Bacillus subtilis*, and the plant *Arabidopsis thaliana* (*8*−*11*).

Vitamin B6 biosynthesis in *B. subtilis* by the so-called alternative route is distinguished from the pathway characterized earlier in *E. coli* as a deoxyxylulose 5-phosphate (DXP)[1] independent pathway (*11*). It comprises only two genes, which encode a highly conserved pyridoxal synthase and glutaminase. These two enzymes, designated Pdx1 (previously termed YaaD) and Pdx2 (previously termed YaaE) in *B. subtilis*, form a high-molecular mass complex containing 24 subunits in total, 12 of each kind. Pdx1 and Pdx2 work in concert and use a pent(ul)ose, either ribose 5-phosphate or ribulose 5-phosphate, and a triose, either glyceraldehyde

† This work was supported by Fonds zur Förderung der wissenschaftlichen Forschung (FWF) Grant PM (17215) and by the European Commission (Grant VITBIOMAL-012158).

* To whom correspondence should be addressed: Institute of Biochemistry, Graz University of Technology, Petersgasse 12/II, A-8010 Graz, Austria. Telephone: +43-316-873 6450. Fax: +43-316-873 6952. E-mail: peter.macheroux@tugraz.at.

‡ Technische Universität Graz.

§ These authors have contributed equally to this work.

|| Biochemiezentrum der Universität Heidelberg.

[1] Abbreviations: C_p, heat capacity; DXP, deoxyxylulose 5-phosphate; DHAP, dihydroxyacetone phosphate; ΔG, Gibbs free energy; ΔH, enthalpy; G3P, glyceraldehyde 3-phosphate; HEPES, 4-(2-hydroxyethyl)piperazine-1-ethanesulfonic acid; IPTG, isopropyl thio-β-D-galactoside; ITC, isothermal titration calorimetry; K_a, association constant; K_d, dissociation constant; MOPS, 4-morpholinepropanesulfonic acid; *N*, stoichiometry; PIPES, piperazine-1,4-bis(2-ethanesulfonic acid); PLP, pyridoxal 5′-phosphate; ΔS, entropy; R5P, ribose 5-phosphate; Ru5P, ribulose 5-phosphate; Tris, 2-amino-2-(hydroxymethyl)-1,3-propanediol.

10.1021/bi602602x CCC: $37.00
Published on Web 04/05/2007

Scheme 1

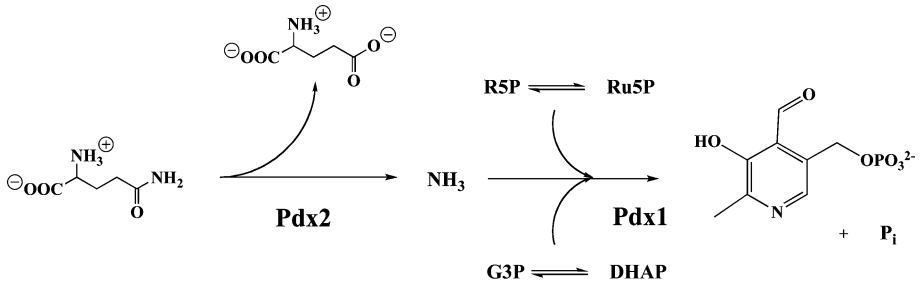

3-phosphate or dihydroxyacetone phosphate, for the generation of the carbon skeleton in PLP. In this reaction, catalyzed by Pdx1, the enzyme incorporates the ammonia produced by Pdx2 using L-glutamine as the source for the required ring nitrogen (Scheme 1).

Previous biochemical studies have indicated that formation of a protein complex between Pdx1 and Pdx2 is required for the catalytic activity of the glutaminase subunit, Pdx2 (*8*, *10*). The recent successful cocrystallization of Pdx1 with a glutaminase deficient Pdx2^{H170N} mutant protein in the presence of L-glutamine led to the structure determination of the ternary complex and to a proposal for how the glutaminase is activated (*12*). The Pdx2^{H170N} mutant protein was necessary for obtaining a substrate complex, and L-glutamine also appeared to stabilize the protein complex as it binds near the heterodimer interface (*12*). The interaction between the two proteins is such that an oxyanion hole, as a requirement for catalysis, forms on the glutaminase, which is obstructed in the structure of the free glutaminase. The biochemical and structural questions that were raised prompted us to engage in a calorimetric study to gain quantitative information about complex formation, using recombinant Pdx1 and Pdx2/Pdx2^{H170N} from *B. subtilis*. In addition, it was our aim to correlate thermodynamic and structural data to better understand the determinants that drive complex formation.

MATERIALS AND METHODS

Reagents. L-Glutamine was from Sigma (Sigma-Aldrich, Vienna, Austria). HEPES, PIPES, MOPS, Tris, imidazole, and NaCl were from Roth (Carl Roth, Karlsruhe, Germany). NaH_2PO_4 was from Merck (Merck KGA, Darmstadt, Germany).

Recombinant Expression, Purification, and Quantification. Pdx1, Pdx2, and Pdx2^{H170N} (His-tagged), cloned into pET21a-(+) (Novagen) and pET24b(+) (Novagen), were expressed in *E. coli* strain BL21(DE3) (Stratagene) at 37 °C. Protein expression was induced at an OD_{600} of 0.6 with IPTG (final concentration of 0.1 mM). After 3 h, bacteria were harvested by centrifugation, washed with 0.9% NaCl, and stored at −20 °C.

For purification of Pdx1, Pdx2, or Pdx2^{H170N}, the cells were thawed and resuspended in lysis buffer [50 mM NaH_2PO_4, 300 mM NaCl, and 10 mM imidazole (pH 8.0)]. The cells were lysed by sonication, and the raw lysate was cleared by centrifugation at 40000*g* for 30 min at 4 °C. The supernatant was applied to a Ni-NTA Sepharose HP column (GE Healthcare), washed with 50 mM NaH_2PO_4, 300 mM NaCl, and 20 mM imidazole (pH 8.0), and eluted with 50 mM NaH_2PO_4, 300 mM NaCl, and 150 mM imidazole (pH 8.0). Fractions containing the protein were combined and dialyzed against 20 mM Tris-HCl and 10 mM NaCl (pH 7.5). The protein was concentrated using Centriprep centrifugal filter devices (Amicon) with a molecular mass cutoff of 10 kDa. Protein concentrations were determined by measuring the absorbance at 280 nm using predicted extinction coefficients of 11 460 (Pdx1) and 2980 M^{-1} cm^{-1} (Pdx2 and Pdx2^{H170N}) (*13*, *14*). The purified proteins were flash-frozen and stored at −20 °C.

Isothermal Titration Calorimetry (ITC). Unless otherwise noted, microcalorimety experiments were carried out in 20 mM Tris-HCl and 10 mM NaCl (pH 7.5). Both the purified enzymes and L-glutamine were dissolved in exactly the same buffer, and all solutions were degassed immediately before measurements were taken. Binding of the titrant (Pdx2 wild-type protein or the Pdx2^{H170N} mutant protein) to Pdx1 in the presence or absence of L-glutamine was analyzed with a VP-ITC microcalorimeter (MicroCal) equilibrated to the respective temperature. The binding of L-glutamine to the individual proteins was tested by ITC using low-*c* value titrations. For this purpose, 100 mM L-glutamine was titrated into 30−50 μM solutions of the individual proteins. Titration of L-glutamine into the Pdx1−Pdx2^{H170N} complex was carried out as a common ITC titration using 1 mM L-glutamine in the syringe and 30 μM protein complex in the measuring cell. In a typical experiment, a total of one aliquot of 2 μL and 29 aliquots of 10 μL of the titrant (250 μM Pdx2 or Pdx2^{H170N}) were injected into 1.421 mL of 30 μM Pdx1 or Pdx1/L-glutamine solution under constant stirring at 310 rpm. All titrations in the absence of L-glutamine were performed with Pdx2 and Pdx2^{H170N}. Every injection was carried out over a period of 20 s in a spacing of 250 s. The heats of binding were determined by integration of the observed peaks. To correct for the heat of dilution of the titrant, the heats evolving in a reference measurement (titrant injected into buffer or L-glutamine) were subtracted from the heat of each injection. The corrected values were plotted against the ratio of the titrant to the protein concentration in the cell to generate the binding isotherm. Nonlinear least-squares fitting with Origin version 7.0 (MicroCal) for ITC data analysis was used to obtain dissociation constants, heats of binding, and stoichiometries. K_d and Gibbs free energy were calculated according to

$$K_d = \frac{1}{K_a} \quad (1)$$

$$\Delta G = -RT \ln K_a = RT \ln K_d \quad (2)$$

Assessment of Proton Transfer Reactions during Protein−Protein Interaction. Purified Pdx1, and Pdx2^{H170N} were

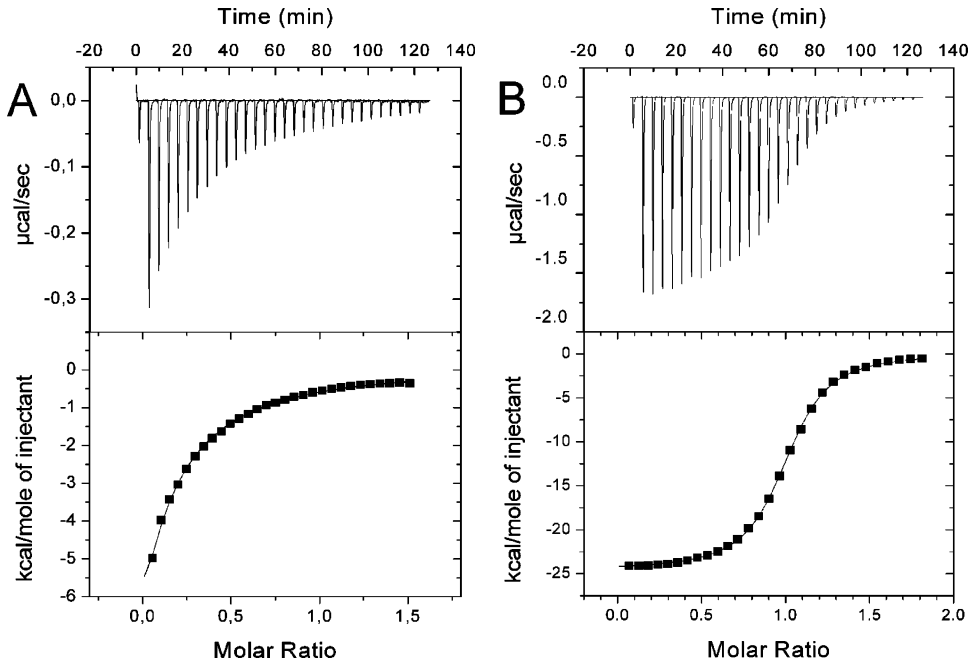

FIGURE 1: Isothermal titration calorimetry of Pdx1 with Pdx2^{H170N} in the absence or presence of L-glutamine. (A) Injection of 250 μM Pdx2^{H170N} into 30 μM Pdx1 in the absence of L-glutamine. (B) Injection of 250 μM Pdx2^{H170N} into 30 μM Pdx1 in the presence of 1 mM L-glutamine. The titrations were performed in 20 mM Tris-HCl and 10 mM NaCl at pH 7.5 and 298 K. The top parts of the panels show the time-dependent release of heat (negative peaks) during the titration. Peak integrals as a function of the molar ratio of Pdx2^{H170N} to Pdx1 are shown in the bottom parts of the panels. The solid curve represents the best fit using a single binding model (for values, see Table 1).

dialyzed against 20 mM PIPES, 20 mM MOPS, or 20 mM Tris (pH 7.5) containing 10 mM NaCl. All experiments were carried out as described for a typical ITC experiment at 25 °C.

Calculation of Accessible Surface Area (ASA). The solvent accessible surface area of the Pdx1−Pdx2 heterodimeric subunit was calculated using the PDB file of the three-dimensional (3D) structural data available in the database (Table 5), and GetArea 1.1 (*15*) or NACCESS (*16*) with the radius of the probe set to 1.4 Å. Theoretical ΔC_p values were calculated from the changes in accessible surface area according to ref *17*.

RESULTS

Formation of the Pdx1−Pdx2 Complex. Formation of a complex between Pdx1 and Pdx2 can be monitored by isothermal microcalorimetry. Titration of Pdx1 with Pdx2 generates a series of exothermic signals that can be used to calculate a dissociation constant of 6.9 ± 1.6 μM at 298 K (25 °C) for the Pdx1−Pdx2 protein complex. It was previously shown that complex formation is favored in the presence of L-glutamine, the amino group nitrogen donor for pyridoxal biosynthesis (*10*). However, titration experiments in the presence of L-glutamine were not successful for the assessment of protein−protein interaction because of the large heat changes associated with the glutaminase activity of Pdx2. Replacement of an essential histidine residue with an asparagine in the active site of Pdx2 leads to complete catalytic inactivation of the glutaminase subunit as shown previously (*12*). Therefore, we have employed this catalytically incompetent glutaminase mutant, designated Pdx2^{H170N}, for our microcalorimetric studies involving L-glutamine (Figure 1A,B). As a control, this mutant protein was used instead of wild-type Pdx2 to determine the dissociation constant of the Pdx1−Pdx2 complex in the absence of L-glutamine. This experiment demonstrated that the single mutation in the active site of Pdx2 has no effect on the formation of the binary Pdx1−Pdx2 complex (data not shown).

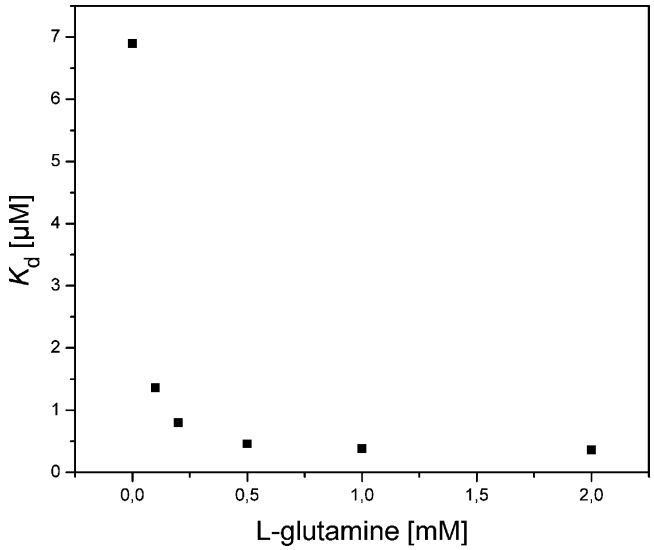

FIGURE 2: L-Glutamine dependency of K_d for formation of the complex between Pdx1 and Pdx2^{H170N}. ITC experiments were performed in 20 mM Tris-HCl and 10 mM NaCl at pH 7.5 and 298 K. In the presence of 0, 0.1, 0.25, 0.5, 1, and 2 mM L-glutmine, 250 μM Pdx2^{H170N} was titrated into 30 μM Pdx1. Every data point represents the average of at least three independent measurements.

Next, we monitored the formation of the Pdx1−Pdx2^{H170N} complex in the microcalorimeter as a function of the concentration of L-glutamine. As shown in Figure 2, increasing the concentration of L-glutamine enhances the affinity of Pdx1 and Pdx2 for complex formation 17-fold, saturating at concentrations above 0.5 mM at a Pdx1 and Pdx 2 concentration of 30 μM (K_d = 0.3 μM at 25 °C). Since the

Table 1: Thermodynamic Parameters for the Binding of Pdx2^{H170N} to Pdx1 in the Absence and Presence of L-Glutamine[a]

	Pdx1−Pdx2^{H170N}					Pdx1−L-glutamine−Pdx2^{H170N}				
	N	Δ*H*	Δ*G*	−*T*Δ*S*	K_d	*N*	Δ*H*	Δ*G*	−*T*Δ*S*	K_d
278 K	0.5 ± 0.03	89 ± 5	−25 ± 2	−111 ± 11	17.8 ± 0.9	1 ± 0.12	4 ± 1	−37 ± 2	−80 ± 4	0.09 ± 0.02
283 K	0.5 ± 0.02	69 ± 26	−26 ± 5	−95 ± 24	22.1 ± 0.7	1 ± 0.06	−14 ± 3	−38 ± 3	−23 ± 4	0.10 ± 0.04
288 K		≈0				1 ± 0.07	−31 ± 3	−39 ± 2	−8 ± 4	0.10 ± 0.02
293 K	0.5 ± 0.12	−13 ± 8	−29 ± 2	−17 ± 9	7.2 ± 0.2	1 ± 0.14	−45 ± 5	−39 ± 2	7 ± 5	0.13 ± 0.03
298 K	0.4 ± 0.10	−34 ± 9	−29 ± 2	9 ± 1	6.9 ± 1.6	1 ± 0.08	−89 ± 12	−37 ± 2	29 ± 2	0.30 ± 0.07
303 K	0.4 ± 0.15	−53 ± 2	−29 ± 1	24 ± 2	9.8 ± 0.9	1 ± 0.14	−78 ± 13	−36 ± 8	42 ± 12	0.52 ± 0.04
308 K	0.4 ± 0.12	−67 ± 18	−30 ± 1	37 ± 18	8.3 ± 0.5	1 ± 0.12	−92 ± 5	−37 ± 5	56 ± 5	0.56 ± 0.03
ΔC_p	−5.5 ± 0.5					−3.21 ± 0.08				

[a] Values are means of at least three experiments. Values of Δ*H*, Δ*G*, and −*T*Δ*S* are in kilojoules per mole. Δ*G* was calculated from the relation $\Delta G = -RT \ln K_a$, where K_a is the association constant determined by ITC. All measurements were performed in 20 mM Tris-HCl and 10 mM NaCl (pH 7.5). The values given for Δ*H* and −*T*Δ*S* are measured values and are not corrected for protonation effects.

Table 2: Binding of L-Glutamine to the Individual Proteins or the Pdx1−Pdx2^{H170N} Complex[a]

protein	*N*	K_d (μM)	Δ***H*** (kJ/mol)	−*T*Δ***S*** (kJ mol^{-1} K^{-1})	Δ***G*** (kJ/mol)
Pdx1			no binding		
Pdx2			no binding		
Pdx2^{H170N}			no binding		
Pdx1−Pdx2^{H170N}	0.5 ± 0.1	11 ± 0.4	−69 ± 11	41 ± 10	−28 ± 6

[a] Values are the average of at least three independent measurements. The concentration of the individual proteins or the Pdx1−Pdx2^{H170N} complex was 30 μM. L-Glutamine (1−100 mM) was titrated into the individual proteins (low-*c* value titration), and 1 mM L-glutamine was titrated into the Pdx1−Pdx2^{H170N} complex. All experiments were carried out in 20 mM Tris-HCl and 10 mM NaCl at pH 7.5 and 298 K.

effect of L-glutamine on protein complex formation is fully developed at a concentration of 1 mM, all further experiments were carried out at this concentration. In addition to its influence on the tightness of the complex, L-glutamine also affects the stoichiometry of complex formation. In the absence of L-glutamine, titration of Pdx1 with Pdx2^{H170N} indicates a stoichiometry (*N*) of 0.5; i.e., only half of the protein−protein docking sites are occupied, whereas in its presence, a stoichiometric 1:1:1 ternary complex is formed (Table 1).

Binding of the Substrate L-Glutamine. In accompanying experiments, we have investigated the binding of L-glutamine to the individual proteins and the binary Pdx1 with Pdx2^{H170N} complex. In principle, low-affinity binding processes can be assessed by low-*c* value microcalorimetric titrations as described in Materials and Methods. The *c* value, also known as Wiseman factor, corresponds to the association constant, K_a, times the concentration of the macromolecule in the cell of the ITC instrument. However, binding of L-glutamine to the individual proteins, Pdx1, Pdx2, or Pdx2^{H170N}, could not be observed under the conditions used in the experiments (Table 2). In contrast, binding to the Pdx1−Pdx2^{H170N} complex produced strong exothermic signals from which a K_d of 11 ± 0.4 μM could be calculated. Titration of L-glutamine to the protein complex is accompanied by a strong loss of entropy, which can be attributed to structural reorganization of the complex induced by binding of L-glutamine to the active site of Pdx2. It should be noted that the stoichiometry for binding of L-glutamine to the preformed complex is also 0.5, suggesting that only half of the binding sites on Pdx2 become occupied. Although it was not possible to observe binding of L-glutamine to Pdx2 directly (see Table 2), a dissociation constant of 260 μM can be calculated from the thermodynamic cycle shown in Scheme 2, assuming full reversibility of the binding processes that are involved.

Temperature Dependence of Thermodynamic Parameters. Formation of a complex between Pdx1 and Pdx2 was further

Scheme 2

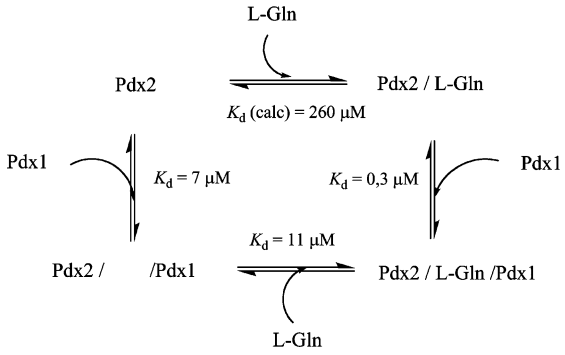

investigated by measuring the thermodynamic parameters as a function of temperature. Parallel experiments were carried out in the absence and presence of L-glutamine (Figure 3 and Table 1). The enthalpic contribution to complex formation showed a linear dependency in both cases (panels A and B). In the absence of L-glutamine, complex formation is driven by a strong contribution from the entropy term below 295 K where the process is endothermic. In contrast to this, complex formation is enthalpy-driven in the presence of L-glutamine with a strong exothermic contribution above 285 K. In summary, formation of the Pdx1−Pdx2^{H170N} complex is entropy-driven (endothermic binding) in the absence of L-glutamine, whereas in its presence, it is mainly enthalpy-driven due to exothermic binding over the entire temperature range investigated with an unfavorable entropic contribution to the free energy of complex formation.

In both cases, the free energy of complex formation (Δ*G*) is nearly constant over the temperature range, showing enthalpy−entropy compensation, a typical phenomenon for aqueous systems. As seen before at 298 K, the free energy of complex formation is significantly more negative in the presence of L-glutamine (see Table 1).

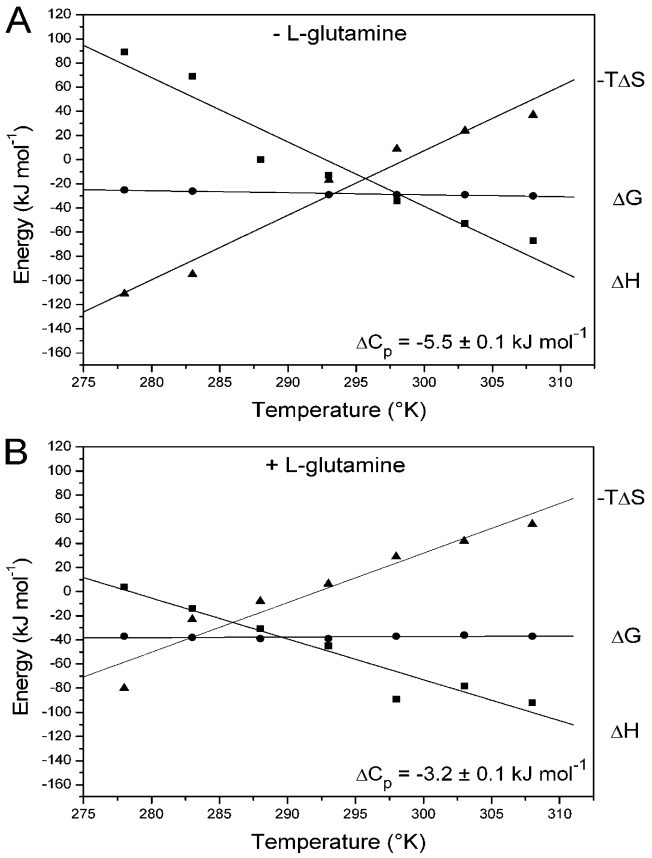

FIGURE 3: Temperature dependency of ΔH (■), $-T\Delta S$ (▲), and ΔG (●) for the binding of Pdx1 and Pdx2^{H170N} in the absence (A) and presence (B) of L-glutamine. Measurements were performed in 20 mM Tris-HCl and 10 mM NaCl at pH 7.5 and various temperatures. (A) Pdx2^{H170N} (250 μM) was titrated into 30 μM Pdx1. (B) Pdx2^{H170N} (250 μM) was titrated into 30 μM Pdx1 in the presence of 1 mM L-glutamine. Experimental ΔC_p values were calculated from the slope of linear regressions to the ΔH data. Each data point represents the average of at least three independent measurements. The values for ΔH and $-T\Delta S$ were not corrected for the observed protonation effects (see Table 4).

The heat capacity change (ΔC_p) of the binding process can be obtained from the slope of the linear temperature dependency of the enthalpy (Figure 3). In both cases, the heat capacity change is negative assuming values of -5.5 ± 0.1 and -3.2 ± 0.1 kJ/mol for complex formation in the absence and presence of L-glutamine, respectively. These large negative heat capacity changes indicate that the Pdx1−Pdx2 interface is dominated by hydrophobic interactions and that the extent and nature of the interaction strongly depend on the presence of L-glutamine in the active site of Pdx2.

Determination of Protonation Enthalpies. Protein−protein interaction may cause conformational changes which in turn may influence the environment of amino acids and hence their pK_a value. Therefore, formation of the Pdx1−Pdx2 complex may be accompanied by an exchange of protons between ionizable groups of amino acid residues and the buffer. Since this process may contribute to the measured enthalpy change (ΔH_{obs}) in the ITC experiment, the observed enthalpies need to be corrected for the ionization enthalpy of the buffer. To accomplish this correction, formation of the Pdx1−Pdx2 complex was analyzed in buffers with different ionization enthalpies, ΔH_{ion} (Figure 4 and Table 3). In the presence of L-glutamine, the slope of the ΔH_{obs} versus ΔH_{ion} plot (Figure 4 and Table 4) is very close to zero, indicating formation of the Pdx1−Pdx2 complex does not involve a net exchange of protons between the proteins and the buffer. In the absence of L-glutamine, the slope of the plot is 0.8, and hence, it is concluded that complex formation involves the uptake of one proton from the buffer (*18*).

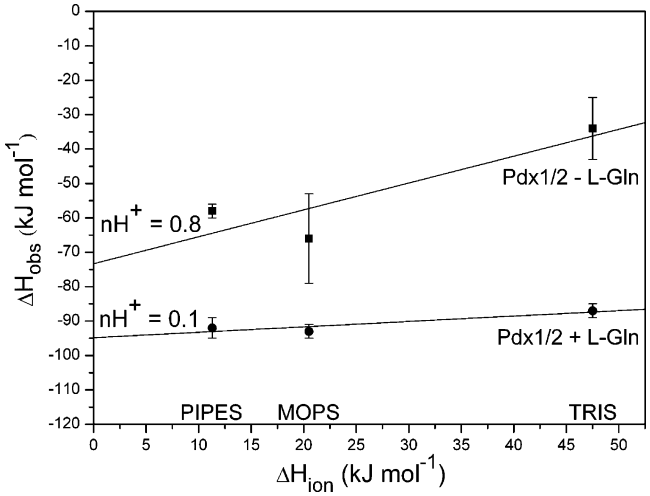

FIGURE 4: Proton transfer reactions accompanying the binding of Pdx1 and Pdx2^{H170N} in the presence (●) and absence (■) of L-glutamine at 298 K. The experimentally observed enthalpy changes, ΔH_{obs}, are plotted against the ionization enthalpy, ΔH_{ion}, of the buffer. The slopes $n[H^+]$ of the linear regressions are given. The ITC experiments were performed in 20 mM PIPES, 20 mM MOPS, or 20 mM Tris (pH 7.5) containing 10 mM NaCl. Each data point represents the average of at least three independent measurements.

Table 3: Protonation Effect Accompanying the Binding of Pdx2 or Pdx2^{H170N} to Pdx1 in the Absence and Presence of L-Glutamine[a]

		ΔH_{obs}	
buffer	ΔH_{ion}[b]	0 mM l-glutamine	1 mM l-glutamine
PIPES	11.3	-58 ± 2	-92 ± 3
MOPS	20.5	-66 ± 13	-93 ± 2
Tris	47.5	-34 ± 9	-87 ± 2

[a] Experiments were carried out in 20 mM PIPES, MOPS, or Tris (pH 7.5) containing 10 mM NaCl. All measurements were performed at 298 K. [b] ΔH_{ion} is the ionization enthalpy of the buffer in kilojoules per mole. Values are means of at least three independent measurements.

Table 4: Buffer Independent Thermodynamic Parameters for the Interaction of Pdx1 and Pdx2^{H170N} in the Absence and Presence of L-Glutamine[a]

	0 mM L-glutamine	1 mM L-glutamine
$n[H^+]$[b]	0.8 ± 0.4	0.11 ± 0.04
ΔH_{bind}[c]	-74 ± 12	-94 ± 1
ΔS_{bind}[c]	149 ± 1	-192 ± 1

[a] All measurements were performed at 298 K. Values are means of at least three independent measurements. [b] Number of protons taken up from buffer during interaction of the proteins. [c] ΔH_{bind} and ΔS_{bind} values are given in kilojoules per mole and joules per kelvin per mole, respectively.

Calculation of Accessible Surface Areas and Heat Capacity Changes. Since both the individual structures of Pdx1 and of Pdx2 as well as a complex of Pdx1 and Pdx2 with bound L-glutamine are available (*12*, *19*), we have calculated the accessible surface areas (ASAs) of the proteins and their complex to obtain the changes in accessible surface areas

Table 5: Changes in Solvent Accessible Surface Area of the Protein Complex

		SASA[a] (Å^2)			ΔSASA[b] (Å^2)		
		polar	apolar	total	polar	apolar	total
GetArea[c]	Pdx1	4799.1	7605.2	12404.3			
	Pdx2/L-Gln	3776.1	5213.1	8989.2			
	Pdx1/2/L-Gln	7497.6	10895.2	18392.8	−1077.6	−1923.0	−3000.6
NACCESS[c]	Pdx1	5059.7	7207.2	12266.8			
	Pdx2/L-Gln	4072.9	4640.3	8682.2			
	Pdx1/2/L-Gln	7973.7	9996.7	17970.4	−1158.9	−1819.8	−2978.6

[a] Solvent accessible surface area (SASA) of the individual proteins (chain A or B of the complex) and the Pdx1/2/L-Gln complex. Chain A (Pdx1) and chain B (Pdx2/L-Gln) or both (Pdx1/2/L-Gln complex) of the Pdx1/2/L-Gln complex structure (PDB entry code 2NV2) were used for the calculations. [b] The change of the solvent accessible surface area (ΔSASA) of the complex was calculated by subtraction of the surface of the proteins from the surface of the Pdx1/2/L-Gln complex. [c] Two different methods were used for the calculation of SASA, GetArea (*15*) and NACCESS (*16*).

Table 6: Experimental and Theoretical ΔC_p Values for the Pdx1−Pdx2−L-Glutamine Complex

		ΔC_p	
	source	GetArea	NACCESS
experimental[a]		−3.21 ± 0.08	
theoretical[b]	Spolar et al. (*23*)	−1.94	−1.76
	Murphy and Friere (*21*)	−2.44	−2.16
	Myers et al. (*24*)	−1.84	−1.69
	Makharadze and Privalov (*20*)	−3.17	−2.88
	Robertson and Murphy (*25*)	−1.83	−1.80

[a] Experimental ΔC_p values were calculated from the slope of linear regression to the ΔH data. [b] Theoretical ΔC_p values were calculated as described in ref *17* according to the respective reference and using the ΔSASA value determined by GetArea or NACCESS (values are listed in Table 5).

(ΔASAs) that occur upon complex formation (Table 5). ASAs were determined using two independent and widely used methods (*15*, *16*). Both calculations yield similar values for polar and apolar surfaces as well as for the changes in accessible surface area occurring during protein complex formation (Table 5). The ΔASA calculations predict that the largest contribution to the buried surface stems from apolar areas (64%), in agreement with the negative heat capacity change determined from the temperature dependence of ΔH (see above). These values were then employed to calculate theoretical heat capacity changes for formation of the Pdx1−Pdx2 complex (Table 6) according to the equation

$$\Delta C_p = \Delta c_{ap}\Delta ASA_{ap} + \Delta c_p \Delta ASA_p \qquad (3)$$

where ΔASA is the apolar (ap) and polar (p) surface buried upon complex formation and Δc is the elementary contribution per square Å of apolar and polar surface in the heat capacity change (*17*). The best agreement to our experimentally determined ΔC_p was obtained using the parameters described in refs *20* and *21*, yielding calculated ΔC_p values of −3.17 and −2.88 kJ mol^{-1} K^{-1} (GetArea and NACCESS) and −2.44 and −2.16 kJ mol^{-1} K^{-1} (GetArea/NACCESS), respectively (Table 6).

DISCUSSION

A recent study of pyridoxal 5′-phosphate (PLP) synthesis by the *B. subtilis* PLP synthase demonstrated the requirement for complex formation of the two components, Pdx1 and Pdx2, in preparing the glutaminase domain Pdx2 for catalysis (*10*). The availability of a high-resolution 3D structure of a Pdx1−Pdx2^{H170N}−L-glutamine ternary complex allowed us to postulate how glutaminase activity is regulated in the complex by oxyanion hole formation (*12*). The structure of the complex prompted us to obtain quantitative thermodynamic data for protein complex formation and to correlate these parameters to the structure of the protein−protein interface formed between Pdx1 and Pdx2. In addition to the structure of the *B. subtilis* PLP synthase, a complex structure of the homologous holoenzyme from *Thermotoga maritima* became recently available (*22*). This PLP synthase complex is different in that it uses a wild-type Pdx2, but there is no L-glutamine bound in the active site of the glutaminase. Nevertheless, the structure of the PLP synthase indicates the formation of a fully developed oxyanion hole; i.e., the glutaminase is primed for catalysis, suggesting that activation of the glutaminase subunit does not necessarily require binding of L-glutamine to the PLP synthase complex.

Initially, we assumed that complex formation is unfavorable in the absence of substrate. Therefore, it was rather surprising to observe binding of Pdx1 and Pdx2 in the low micromolar range (6.9 μM at 25 °C) in our ITC experiments. Using the catalytically inactive Pdx2^{H170N}, it could be shown that the dissociation constant of the Pdx1−Pdx2 complex decreases 17-fold in the presence of L-glutamine (0.3 μM at 25 °C). Binding of L-glutamine to the individual proteins could not be detected in our microcalorimetry experiments, however, the dissociation constant for binding of L-glutamine to Pdx2 can be calculated on the basis of the thermodynamic cycle shown in Scheme 2. The value obtained from this calculation is 260 μM, roughly 4 times lower than the previously reported K_M for this substrate [1 mM (*10*)]. This indicates that the rate of subsequent chemical steps contributes significantly to the Michaelis−Menten parameter.

In addition to the effect on the complex dissociation constant, we also observed an influence on the stoichiometry of the complex. In the absence of L-glutamine, titration of Pdx1 with Pdx2 yields a stoichiometry (N) of 0.5 for the binary protein−protein complex, whereas in the presence of L-glutamine, the stoichiometry reaches unity. This indicates that L-glutamine has a direct effect on the occupation of the docking sites on Pdx1. Strohmeier et al. (*12*) demonstrated recently that Pdx1 in solution occurs as a dodecamer in equilibrium with a hexamer ($K_d \approx 3.7$ μM), shifting entirely toward the dodecamer in the presence of Pdx2^{H170N} and L-glutamine. If the two oligomeric states of Pdx1 have different affinities for Pdx2, this could give rise to substoichiometric binding of Pdx2 to Pdx1. However, since our ITC experiments were performed at a Pdx1 concentration

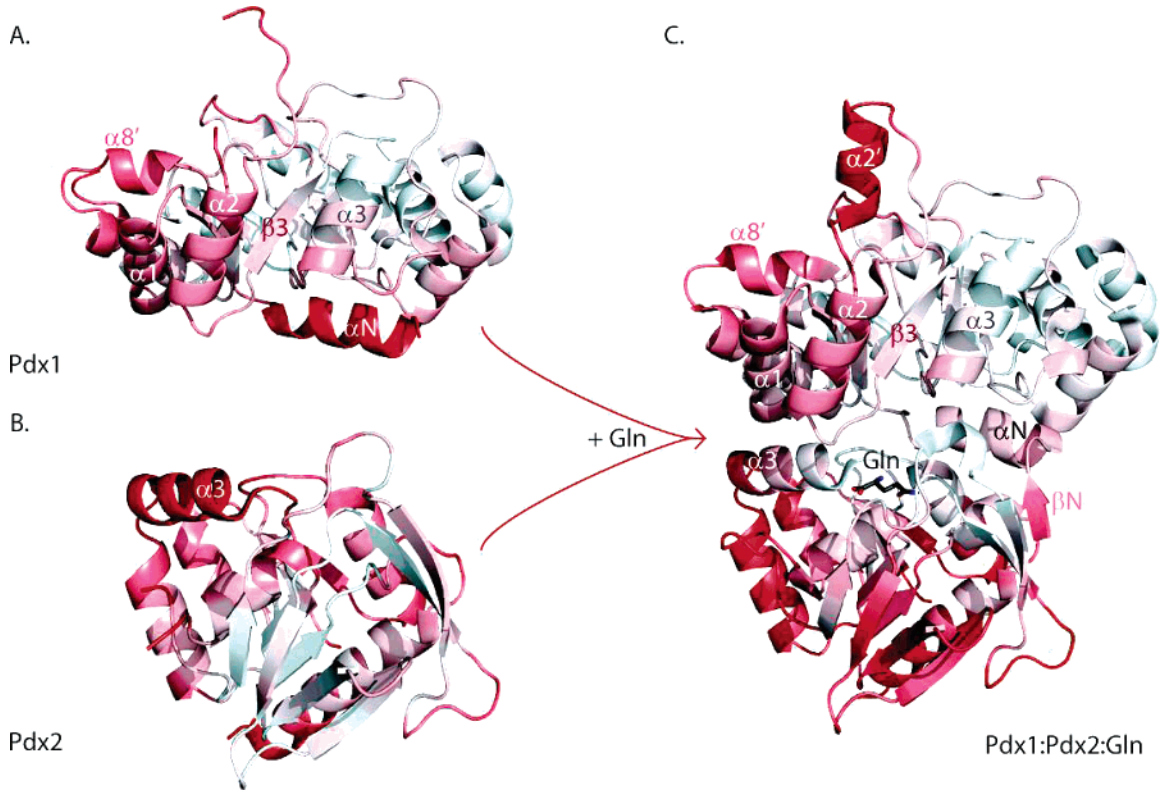

FIGURE 5: Secondary structure representation of free Pdx1 (A), free Pdx2 (B), and Pdx1 in complex with $Pdx2^{H170N}$ (C). The structures are colored according to their *B*-factors by running a pymol script as provided by R. L. Campbell with enhancements from J. Stroud on http://adelie.biochem.queensu.ca/~rlc/work/pymol/. White-colored regions indicate a *B*-factor lower than the average *B*-factor, whereas red regions indicate a *B*-factor above average. L-Glutamine is shown in a stick representation with oxygen colored red and nitrogen colored blue.

that is ~10-fold higher than the K_d for the dodecamer−hexamer equilibrium, we can safely assume that Pdx1 is predominantly present in the dodecameric state, and hence, this rationale cannot be applied to explain our experimental data. Instead, we propose that Pdx2 occupies only half of the docking sites on the dodecameric Pdx1 and that the binding of L-glutamine to Pdx2 triggers structural changes in the Pdx1 dodecamer, which leads to full occupancy of the available docking sites. In this context, it is important to note that L-glutamine needs to bind to Pdx2 first because the preformed Pdx1−Pdx2 "encounter complex" also responds with a lower stoichiometry to the addition of L-glutamine (see Table 2).

A more detailed analysis of the temperature dependency revealed that the interactions in the Pdx1−Pdx2 complex interface depend on the presence of the substrate L-glutamine. Although the dissociation constant for the complex remains nearly constant over the examined temperature range (see Table 1), the enthalpic and entropic contributions to binding depend on the presence of L-glutamine. In the absence of L-glutamine, binding is endothermic at lower temperatures, and hence, complex formation is largely driven by an increase in entropy. In contrast to this, binding is exothermic over most of the observed temperature range in the presence of L-glutamine with a smaller contribution from the entropy term. This can be interpreted in terms of a greater structuring of the complex in the presence of L-glutamine as compared with the substrate-free complex.

This conclusion is corroborated by an analysis of the heat capacity changes (ΔC_p) observed for complex formation in the absence and presence of L-glutamine (Figure 3 and Table 1). Both ΔC_p values (slope of ΔH vs T) are negative, indicating that complex formation is associated with the dehydration of apolar areas in Pdx1 and Pdx2, and hence, apolar interactions dominate in the complex interface (Table 5). However, the heat capacity change is almost twice as large in the absence of L-glutamine as compared to its presence, suggesting that apolar interactions are even more dominant in the substrate-free Pdx1−Pdx2 complex. In other words, the relative contribution of polar interactions is higher in the protein complex when L-glutamine is bound to the active site of Pdx2. Furthermore, the finding that a net protonation event is observed in the absence of L-glutamine also points toward a compositional change in the complex interface (Figure 4).

We were also interested in comparing our experimental heat capacity changes with values obtained from theoretical calculations. Toward that end, we have used the protein structures determined by X-ray crystallography to calculate the accessible surface areas (ASAs) and the changes occurring upon protein complex formation (Table 5). The best fit to the experimental heat capacity change was found with models that assume a high positive value for the area coefficient for apolar and a high negative area coefficient for polar contributions (Table 6). From eq 3, we can also interpret the more negative heat capacity change for complex formation in the absence of L-glutamine in terms of a smaller contribution of $\Delta c_p \Delta ASA_p$ relative to $\Delta c_{ap} \Delta ASA_{ap}$; i.e., more apolar surface is buried relative to polar surface in the substrate-free complex. In the absence of a 3D structure of the ligand-free *B. subtilis* Pdx1−Pdx2 complex, a comparison with the ligand-free *T. maritima* PLP synthase structure

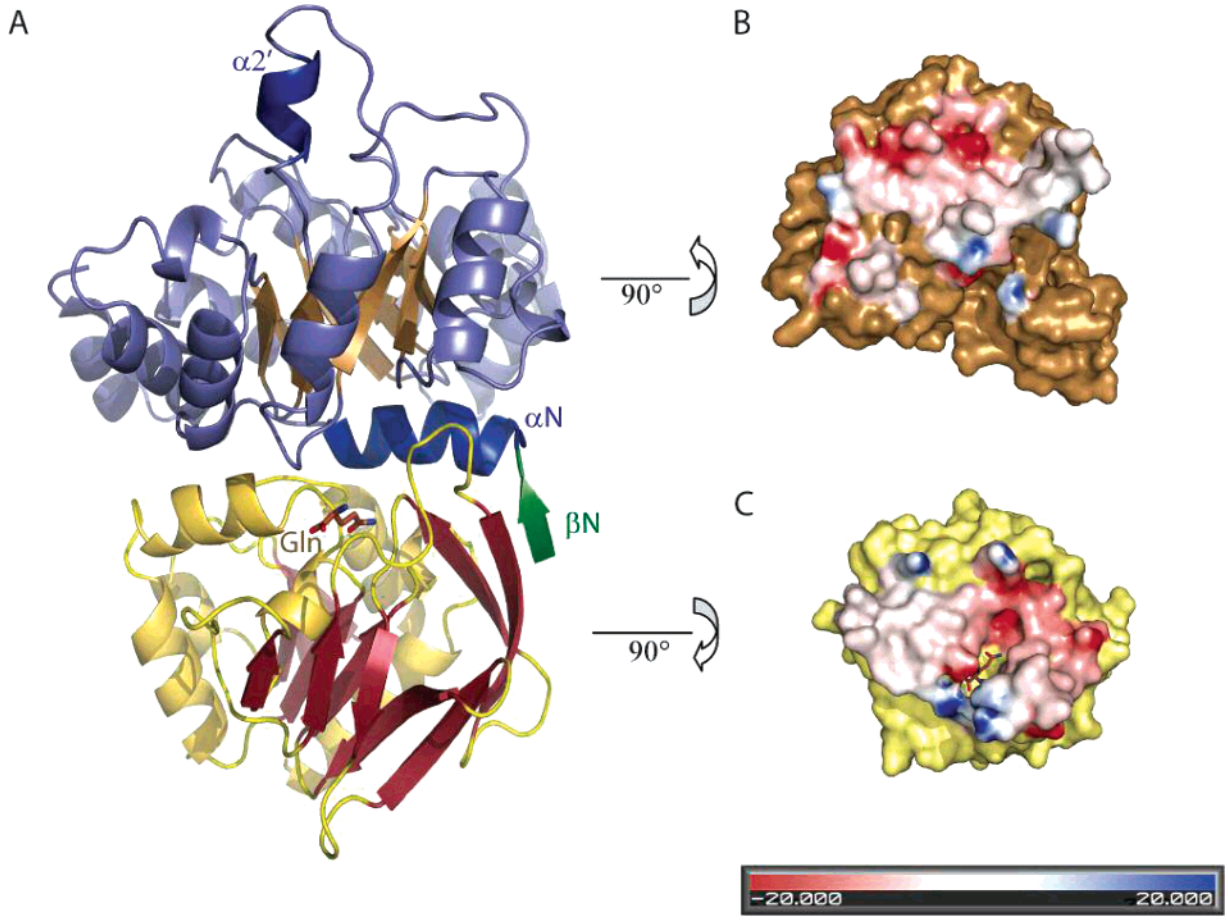

FIGURE 6: (A) Heterodimeric complex of *B. subtilis* Pdx1 (blue and green) and Pdx2^{H170N} (yellow and red) in the presence of L-glutamine (brown, oxygen atoms colored red and nitrogen atoms blue). The interface forming helix αN and the N-terminal *β*-strand *β*N, only visible in the complex structure, are highlighted in darker blue and green, respectively. α-Helix α2′, only observed in the structure of the Pdx1−2^{H170N} complex, has also been highlighted in darker blue. (B) Surface representation of Pdx1 rotated by 90° around the indicated axis in comparison to panel A. The part of the surface interacting with Pdx2^{H170N} is colored according to the electrostatic potential, as calculated with GRASP. The area that is not in contact with Pdx2^{H170N} is colored brown. (C) Surface representation of Pdx2^{H170N} colored in the same way as Pdx1 in panel B. In comparison to panel A, Pdx2^{H170N} has also been rotated by 90° as indicated by the arrow. The residues in each monomer interacting with residues of the binding partner were identified using CONTACT (distance parameters of 0−4 Å), a program implemented in the ccp4 program suite (*26*). Pymol was used to prepare the figures (*27*).

would suggest that no structural changes occur on substrate binding. This in turn then requires that the differences be due solely to the changed interface when L-glutamine is present.

The available crystal structure of the Pdx1−Pdx2−L-glutamine ternary complex offers an opportunity to outline correlations to our thermodynamic data. The focus of our interest revolved around two main issues: (i) the structuring of the proteins upon complex formation as indicated by the observed loss of entropy and (ii) the nature of the complex interface. As far as the first point is concerned, comparison of the Pdx1−Pdx2 complex and the autonomous Pdx1 structure reveals the ordering of the N-terminus of Pdx1, most notably the engagement of the N-terminal amino acids (amino acids 2−6) in *β*-completion with *β*7 and *β*8 of Pdx2 and the ordering of an α-helix (designated helix αN in Figure 5) at the center of the interface (*12*). As illustrated in Figure 5, the *B*-factors of helix αN decrease significantly upon complex formation (compare panels A and C), indicating a loss of translational, vibrational, and rotational freedom of the amino acid residues. This α-helix was found to cover the entire length of the active site of Pdx2 engaging in salt bridges at both ends with a hydrophobic patch in the more central part of the α-helix (Figure 6C). In addition, a small *β*-sheet is formed upon complex formation, which is absent in the autonomous Pdx1 structure. The essential role of αN and *β*N for complex formation was demonstrated by a Pdx1 deletion mutant protein lacking 18 amino acids at the N-terminus, which was unable to form a complex with Pdx2 (*12*). Because L-glutamine appears to have a pivotal role in the structuring of the N-terminal amino acids of Pdx1, we assume that it occurs only in the ternary Pdx1−Pdx2−L-glutamine complex but not in the binary Pdx1−Pdx2 complex. Therefore, the unfavorable entropic contribution to formation of the ternary complex can be attributed to the ordering of the N-terminal segment of Pdx1 and also to helix α2′ on the opposite side of the interface (Figure 6).

The formation of the binary and ternary complex is associated with a negative heat capacity change indicative of the dominance of apolar interactions in the complex interface. However, the heat capacity change is less negative for the formation of the ternary complex, suggesting that the relative contribution of apolar contributions is smaller. Inspection of the complex interface in the presence of L-glutamine, as depicted in Figure 6 (panels A and B), reveals that the contact area between Pdx1 and Pdx2 is dominated

by hydrophobic interactions (64%) with polar interactions contributing only 36% (see also Table 5). It would follow from these considerations that apolar interactions contribute even more to the complex interface in the absence of L-glutamine. Since the N-terminal amino acids appear to play an important role in Pdx1−Pdx2 binding, as demonstrated by the effect of the Δ18-Pdx1 mutant protein, it is proposed that these amino acids form a hydrophobic patch with apolar amino acids at the surface of Pdx2. This assumption is supported by the hydropathy index of the N-terminus of Pdx1; however, their interaction partners on the surface of Pdx2 remain unidentified in the absence of structural data. In any case, binding of L-glutamine to Pdx2 triggers the ordering of the N-terminus as discussed above and shifts the contributions to the complex interface toward more polar interactions, i.e., causes the dissolution of hydrophobic patches, suggested to involve the N-terminal amino acids of Pdx1. From these considerations, we conclude that L-glutamine induces the correct alignment in the protein interface such that PLP synthesis can occur in the Pdx1−Pdx2 protein complex, or in other words, the initial encounter complex of Pdx1 and Pdx2 is transformed into a catalytic complex in which the pertinent amino acid residues are aligned to act on the substrate. It will be interesting to see whether the binding of the pentose and triose to Pdx1 has similar effects on protein complex formation as suggested by the recent complex structure of the *T. maritima* PLP synthase (*22*). Our future efforts will now focus on individual amino acid residues in the complex interface with the aim of determining their contribution to complex formation.

ACKNOWLEDGMENT

We thank Dr. Teresa Fitzpatrick (ETH Zürich, Zürich, Switzerland) for the generous gift of the expression plasmids for Pdx1, Pdx2, and Pdx2^{H170N}.

REFERENCES

1. Eliot, A. C., and Kirsch, J. F. (2004) Pyridoxal phosphate enzymes: Mechanistic, structural and evolutionary considerations, *Annu. Rev. Biochem. 73*, 383−415.
2. John, R. A. (1998) *Pyridoxal phosphate dependent enzymes*, Academic Press, San Diego.
3. Cane, D. E., Du, S. C., Robinson, J. K., Hsiung, Y., and Spenser, I. D. (1999) Biosynthesis of vitamin B-6: Enzymatic conversion of 1-deoxy-D-xylulose-5-phosphate to pyridoxol phosphate, *J. Am. Chem. Soc. 121*, 7722−7723.
4. Laber, B., Maurer, W., Scharf, S., Stepusin, K., and Schmidt, F. S. (1999) Vitamin B6 biosynthesis: Formation of pyridoxine 5′-phosphate from 4-(phosphohydroxy)-L-threonine and 1-deoxy-D-xylulose-5-phosphate by PdxA and PdxJ protein, *FEBS Lett. 449*, 45−48.
5. Ehrenshaft, M., Bilski, P., Li, M. Y., Chignell, C. F., and Daub, M. (1999) A highly conserved sequence is a novel gene involved in *de novo* vitamin B6 biosynthesis, *Proc. Natl. Acad. Sci. U.S.A. 96*, 9374−9378.
6. Osmani, A. H., May, G. S., and Osmani, S. A. (1999) The extremely conserved *pyro*A gene of *Aspergillus nidulans* is required for pyridoxine synthesis and is required indirectly for resistance to photosensitizers, *J. Biol. Chem. 274*, 23565−23569.
7. Mittenhuber, G. (2001) Phylogenetic analyses and comparative genomics of vitamin B6 (pyridoxine) and pyridoxal phosphate biosynthesis pathways, *J. Mol. Microbiol. Biotechnol. 3*, 1−20.
8. Belitsky, B. R. (2004) Physical and enzymological interaction of *Bacillus subtilis* proteins required for de novo pyridoxal 5′-phosphate biosynthesis, *J. Bacteriol. 186*, 1191−1196.
9. Dong, Y.-X., Sueda, S., Nikawa, J.-I., and Kondo, H. (2004) Characterization of the products of the genes *SNO1* and *SNZ1* involved in pyridoxine synthesis in *Saccharomyces cerevisiae*, *Eur. J. Biochem. 271*, 745−752.
10. Raschle, T., Amrhein, N., and Fitzpatrick, T. B. (2005) On the two components of pyridoxal 5′-phosphate synthase from *Bacillus subtilis*, *J. Biol. Chem. 280*, 32291−32300.
11. Tambasco-Studart, M., Titiz, O., Raschle, T., Forster, G., Amrhein, N., and Fitzpatrick, T. B. (2005) Vitamin B6 biosynthesis in higher plants, *Proc. Natl. Acad. Sci. U.S.A. 102*, 13687−13692.
12. Strohmeier, M., Raschle, T., Mazurkiewicz, J., Rippe, K., Sinning, I., Fitzpatrick, T. B., and Tews, I. (2006) Structure of a bacterial pyridoxal 5′-phosphate synthase complex, *Proc. Natl. Acad. Sci. U.S.A. 103*, 19284−19289.
13. Mach, H., Middaugh, C. R., and Lewis, R. V. (1992) Statistical determination of the average values of the extinction coefficients of tryptophan and tyrosine in native proteins, *Anal. Biochem. 200*, 74−80.
14. Pace, C. N., Vajdos, F., Fee, L., Grimsley, G., and Gray, T. (1995) How to measure and predict the molar absorption coefficient of a protein, *Protein Sci. 4*, 2411−2423.
15. Fraczkiewicz, R., and Braun, W. (1998) Exact and efficient analytical calculation of the accessibel surface areas and their gradients for macromolecules, *J. Comput. Chem. 19*, 319−333.
16. Hubbard, S. J., and Thornton, J. M. (1996) *NACCESS Computer Program*, version 2.1.1, Department of Biochemistry and Molecular Biology, University College, London.
17. Prabhu, N. V., and Sharp, K. A. (2005) Heat capacity in proteins, *Annu. Rev. Phys. Chem. 56*, 521−548.
18. Baker, B. M., and Murphy, K. P. (1998) Prediction of binding energetics from structure using empirical parameterization, *Methods Enzymol. 295*, 294−315.
19. Bauer, J. A., Bennett, E. M., Begley, T. P., and Ealick, S. E. (2004) Three-dimensional structure of YaaE from *Bacillus subtilis*, a glutaminase implicated in pyridoxal-5′-phosphate biosynthesis, *J. Biol. Chem. 279*, 2704−2711.
20. Makharadze, G. I., and Privalov, P. L. (1995) Energetics of protein structure, *Adv. Protein Chem. 47*, 307−425.
21. Murphy, J. K., and Freire, E. (1992) Thermodynamics of structural stability and cooperative folding behavior in proteins, *Adv. Protein Chem. 43*, 313−361.
22. Zein, F., Zhang, Y., Kang, Y.-N., Burns, K., Begley, T. P., and Ealick, S. E. (2006) Structural insights into the mechanism of the PLP synthase holoenzyme from *Thermotoga maritima*, *Biochemistry 45*, 14609−14620.
23. Spolar, R. S., Livingstone, J. R., and Record, M. T. (1992) Use of liquid hydrocarbon and amide transfer data to estimate contributions to thermodynamic functions of protein folding from the removal of nonpolar and polar surface from water, *Biochemistry 31*, 3947−3955.
24. Myers, J. K., Pace, C. N., and Scholtz, J. M. (1995) Denaturant m values and heat capacity changes: Relation to changes in accessible surface areas of protein unfolding, *Protein Sci. 4*, 2138−2148.
25. Robertson, A. D., and Murphy, K. P. (1997) Protein structure and the energetics of protein stability, *Chem. Rev. 97*, 1251−1267.
26. Collaborative Computational Project Number 4 (1994) The CCP4 suite: Programs for protein crystallography, *Acta Crystallogr. D50*, 760−763.
27. Delano, W. L. (2002) *The PyMOL molecular graphics system*, DeLano Scientific, San Carlos, CA.

BI602602X